IEEE Open Journal of
Industry Applications

Received 3 September 2020; revised 12 November 2020; accepted 2 December 2020. Date of publication 7 December 2020;
date of current version 21 December 2020. The review of this article was arranged by Associate Editor Dr. Shafiq Odhano.

Digital Object Identifier 10.1109/OJIA.2020.3042884

Analysis, Design and Optimization of Hysteresis Clutches

GIANVITO GALLICCHIO [1] (Member, IEEE), MAURO DI NARDO [2] (Member, IEEE), MARCO PALMIERI [1] (Member, IEEE), AND FRANCESCO CUPERTINO [1] (Senior Member, IEEE)

[1] Department of Electrical Engineering and Information Technology, Politecnico di Bari, 70 126, Bari Italy
[2] Power Electronics and Machine Control Group, University of Nottingham, Nottingham NG7 2RD, U.K.

CORRESPONDING AUTHOR: GIANVITO GALLICCHIO (e-mail: gianvito.gallicchio@poliba.it)

ABSTRACT Electromagnetic clutches are widely used devices in industrial applications when a torque must be transmitted between two components without mechanical contact avoiding friction and so reducing wear and maintenance time. Hysteresis clutches are a particular variant of electromagnetic couplers used when a constant torque from zero to the synchronous speed needs to be transmitted. This paper deals with the analysis, design and optimization of hysteresis clutches. After a brief introduction on the operating principle, a new method of analysis is then introduced. The latter allows a fast prediction of the performance of hysteresis couplers without sacrificing the accuracy of the performance evaluation even when adopting anisotropic magnetic materials. The introduced method, based on a static finite element simulation followed by a post-processing of the evaluated magnetic field, is then used within an automatic design procedure in order to identify the inevitable trade-offs encountered when optimizing the geometry of any hysteresis clutches with a given outer envelope. The obtained results are commented in-depth and allow to draw general design guidelines with special regards to the selection of the number of poles and the magnetic materials. The effect of the high level of anisotropy of the most common magnetic materials showing the highest energy density is carefully taken into account allowing to deduce the optimal preferred direction of magnetization.

INDEX TERMS Alnico, design optimization, electromagnetic coupler, finite element analysis, hysteresis clutch, hysteresis model.

I. INTRODUCTION

In many areas of engineering mechanical or electromagnetic clutches are used in order to separate parts in relative motion. Mechanical clutches are the most common solution, both in automotive and industrial applications. These systems require continuous maintenance and present a low efficiency [1]. Conversely the electromagnetic clutches are able to transmit the torque without contact between the parts in relative motion avoiding problems related with the wear, reducing the mechanical vibrations and permitting a higher level of misalignment between the coupled shafts [2]. As for electric motors, it is possible to discern between synchronous and asynchronous types of electromagnetic couplers. Hysteresis clutches present an interesting feature because they are capable of transmitting torque in both operating conditions (i.e asynchronous and synchronous). The operating principle of a hysteresis clutch is similar, but not identical, to a hysteresis motor. The latter produces an electromagnetic torque proportional to the hysteresis losses in the rotating part of the machine, as first described by Steinmetz in [3]. The hysteresis motor is composed by a conventional slotted stator hosting a distributed winding and a rotor made of a ring of semi-hard or hard ferromagnetic material, such as AlNiCo, sustained by a shaft which can be either magnetic or non-magnetic. The drawbacks of this kind of electrical machines are the really poor power density and power factor and these are the reasons of their adoption only in niche applications [4]. However, due to its simple rotor structure, this kind of machine is attracting more and more attention for applications with extremely high rotational speed [4] and for applications requiring a self-starting capability [5]. A hysteresis clutch, from a structural point of view, is composed by two coaxial rings. Rare earth based permanent magnets or electromagnets are housed on one of the two rings and

constitute the magnetic field generator. The other ring is made of semi-hard or hard ferromagnetic material and constitutes the "hysteresis" ring. In the following, the inner ring is considered to be made of NdFeB magnets, whereas the hysteresis ring is made of AlNiCo. The latter is the most used one in hysteresis machines, due to its large hysteresis loop. Many grades of AlNiCo are available according to the value of the coercive field. The lower grades (i.e 2, 3 and 4) are unoriented, i.e. the magnetic properties are the same in all directions. Higher grades (i.e 5, 6, 7, 8, 9) are anisotropic so a preferred direction of magnetization/orientation exists. While hysteresis motors are not widely used in industrial applications, the hysteresis clutches are commonly used along with the classic synchronous clutches. In the latter both rings are made of an array of rare earth permanent magnets. The different working principles of these two types of clutches obviously lead to a completely different torque-speed behavior. In fact, synchronous clutches produce torque proportional to the sine of angular displacement between the magnetic pole axis of the inner and outer rings only when the speeds of both rings are the same. In asynchronous condition the electromagnetic torque is on average zero but it is not constant and features large oscillations. On the contrary, hysteresis clutch produces the same torque from zero to synchronous speed with a limited torque ripple [6].

The design of hysteresis motors and clutches has been the subject of few contributions in the literature. Analytical approaches are reported in [7], [8] and they are based on approximations of the problem formulation. Conversely, [9]–[11] propose a numerical method based on finite element analysis and vector hysteresis model, and use an iterative procedure to calculate the hysteresis torque with really high computational burden.

The first goal of this work is to present an accurate and fast method of analysis of hysteresis clutches based on finite element analysis and a post-processing of the evaluated magnetic field in the hysteresis region. The method for the computation of the machine performances was first proposed in [12] and here is extended in order to consider the anisotropic behaviour of the highest grades of AlNiCo, i.e. the ones that usually feature the highest energy density [13]. A design optimization procedure employing the introduced performance evaluation method is then proposed and used to obtain design guidelines of hysteresis clutches. Particular attention will be posed to the selection of the number of poles of the NdFeB ring and the AlNiCo grade since both have significant effects on the optimal geometry and on the performances of a hysteresis clutch. It will be shown the paramount importance of considering the anisotropic behaviour of the AlNiCo when analysing and designing hysteresis clutches. Disregarding such effect would lead to incorrect performance estimation and more importantly to sub-optimal design solutions.

The paper is organized as follows. The operating principle of a hysteresis machine is described in Section II. In Section III, a brief literature review is reported along with the method for the computation of the machine performances. Section IV reports the design optimization procedure, whereas the optimization results are shown in Section V. Finally, the main conclusions are summarized in the last section.

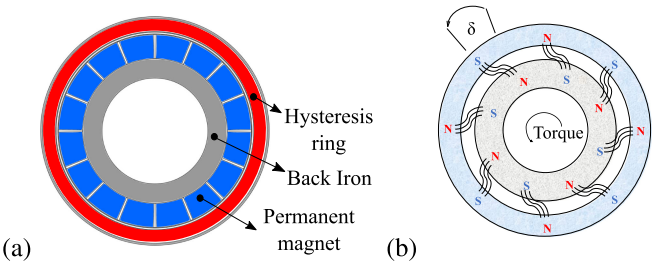

FIGURE 1. (a) Hysteresis clutch typical configuration, (b) operating principle.

II. OPERATING PRINCIPLE

In Fig. 1(a) is reported a typical hysteresis clutch. The inner ring is composed by permanent magnets, whereas the outer ring is made by hard ferromagnetic material (HFM). When the inner ring starts rotating, a rotating magnetic field is established in the airgap. Due to the hysteresis behaviour, the flux density in the HFM lags behind the magnetic field, and this shift angle between the magnetic field (H) and the flux density (B) generates a torque. From a qualitative point of view, the inner ring field generates poles on the outer ring. These induced poles follow the rotating field and pull the outer ring along, as shown in Fig. 1(b). The maximum torque, which is also called pull-out torque [14], can be written as :

$$T_{hys} = \frac{pV}{2\pi} \oint \mathbf{B} d\mathbf{H} \tag{1}$$

where p is the number of pole pairs, $\mathbf{B}$ is the flux density, $\mathbf{H}$ is the magnetic field intensity and V is the volume of the HFM region. The torque, which is the maximum one that the clutch can transmit during synchronous operation, is ideally speed independent in the asynchronous range (i.e inner ring speed different with respect to the outer ring one). Nevertheless, in reality the torque also depends on the slip, i.e on the differences between the outer and the inner ring speeds. In fact, eddy currents arising in both rings generate a torque component directly proportional to the slip. As a consequence, the actual asynchronous torque is not constant with respect to the slip and it decreases until the synchronous speed is reached. Usually this speed dependent effect of the torque is neglected (being at most 10% according to the electric resistivity of the HFM, [15], [16]) either because it is numerically negligible or because the design aimed at minimizing it. If otherwise, the main benefit of this clutch type, i.e. the capability to transmit constant torque within the speed range of interest, would vanish. When the synchronous speed is reached, the outer ring remains magnetized and the clutch behaves as a synchronous clutch. Consequently, the synchronous torque is load dependent. In particular, if the load torque is less than the maximum one expressed in (1), the outer ring angular speed will increase with respect to the inner ring until the torque,

which depends on the shift angle, balances the load torque. In this operating scenario, as pointed out in [15], if the applied torque is smaller than the value expressed in (1), the involved mechanical energy is not enough to change the magnetization state of the HFM which behaves as a permanent magnet. Conversely, if the load torque is higher than the maximum one, the outer ring will decelerate until it stops and the torque will remain constant. So, a hysteresis clutch can be defined as a synchronous coupler if the load torque is less than pullout value, whereas the clutch operates as an asynchronous coupler if the load torque exceeds the same value.

III. MODELING TECHNIQUE

A. LITERATURE REVIEW

In [7], [8], [17] analytical approaches to compute the performances of hysteresis machines are proposed. These methods are applied to idealized machines where no saturation effect is considered and the hysteresis loops (i.e major and minor loops) are modelled using elliptical or parallelogram shapes. In addition, the dependence of the coercive force by the operating point is not modelled whereas the permeability of the magnetic yokes is assumed to be infinite and the flux density in the hysteresis region is assumed independent of the radius. These approaches are very useful to provide a first approximation of the performances of the machine and so they are usually followed by a FE simulation employed to refine the performance evaluation. Most of the commercial available FE software use a single value BH curve to perform the FE analysis therefore the hysteresis losses are usually calculated post-processing the magnetic field. Few FE suites, [18], [19], take into account the hysteresis behaviour of the materials within the FE evaluation allowing a direct and more precise calculation of the hysteresis losses and related torque. The first suite [18] uses the model presented in [20], whereas the latter implements the Jiles-Atherton model [21]. Other ways [9]–[11], [14] to determine the hysteresis losses/torque consists in performing the finite element analysis with the single value BH curve and post-processing the magnetic field using hysteresis model, such as Preaich models [22], [23] or Jiles-Atherton model in an iterative fashion. In particular, in [9] a linear finite element analysis is performed initially assuming an arbitrary permeability and magnetization in each element of the hysteresis region. The maximum value of the circumferential component of the flux density is then extracted and the related hysteresis loop is constructed using the Preisach model. Then, the operating point (i.e the actual value of the magnetization and the magnetic field intensity) is evaluated along with the updated value of the permeability of each hysteresis element. A new FEA is then performed and the procedure continues until a convergence criterion is satisfied. Conversely, in [10], first a non-linear finite element analysis is carried out. From the field solution, the characteristics of an equivalent hysteresis loop of elliptical shape are extracted and form the input of the steady-state analysis aimed at finding the best inclined ellipse in various current levels based on the predetermined desired error. Although all interesting, the main drawback of mentioned methods is the high computational burden and the consequent difficulty of being embedded in automatic design procedures.

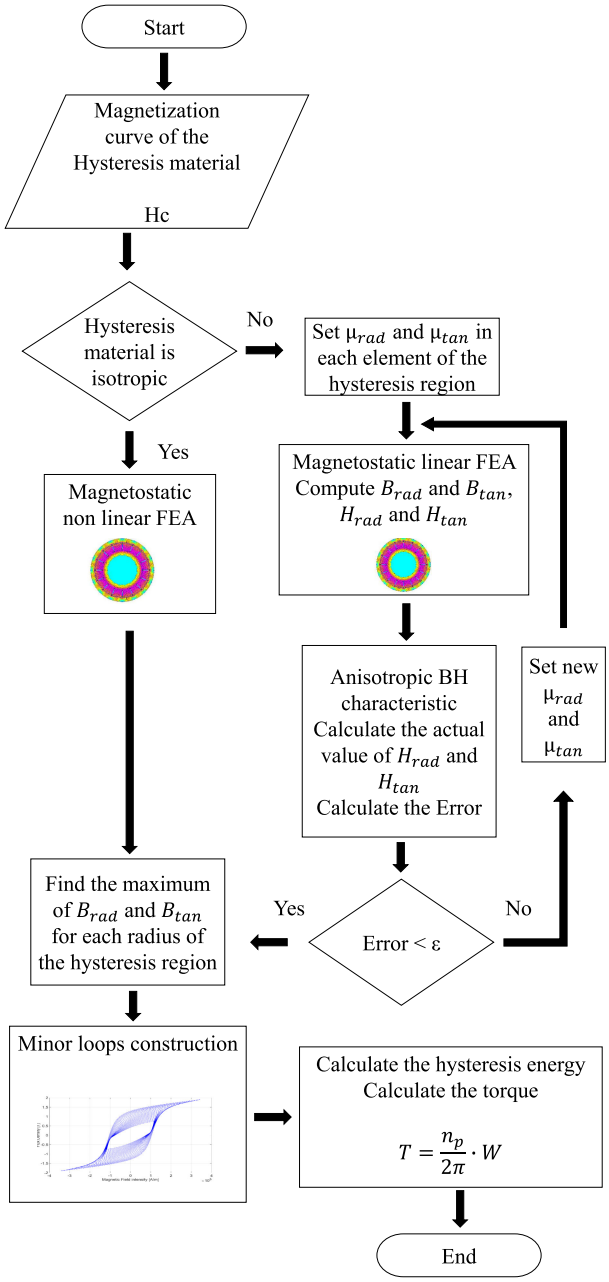

FIGURE 2. Flowchart of the proposed hybrid method for the torque computation.

B. PROPOSED METHOD OF ANALYSIS

Fig. 2 reports a flowchart of the implemented performance evaluation procedure. The method is based on a non-linear magneto-static FEA and a post-processing of the magnetic field in the hysteresis region (hereafter called hysteresis model). The finite element analysis, performed with FEMM [24], does not implement a vector hysteresis model

but uses a single value BH curve of each materials thus allowing to relieve the computational burden respect to the more complex FE implementation of vector hysteresis models. The implemented post-processing hysteresis model consists in lookup table, in which the flux densities computed by FEA (in the radial and circumferential directions) in the hysteresis region are the input and the mean torque is the output. The procedure depends on the type of the HFM and it is necessary to discern between the isotropic and anisotropic case.

- Isotropic case: the hysteresis region can be defined by its non-linear *BH* curve in the finite element formulation (2)

$$\mathbf{B} = f(\mathbf{H}) \tag{2}$$

  where H is the magnetic field intensity in the hysteresis region and B is the flux density in the hysteresis region. The method needs only one magneto-static simulation, which lasts at most 2 seconds and the post-processing hysteresis model is the same both in the radial and in the circumferential direction.
- Anisotropic case: the radial *BH* curve and the circumferential one are different, as well as the post-processing hysteresis models. Since FEMM does not allow to define a non-linear anisotropic material, an iterative method has been implemented. In the first iteration step, all the elements of the hysteresis region are set to have a unit relative permeability in the radial direction and in the circumferential direction, μ_{rad} and μ_{tan} (3)

$$\begin{aligned} B_{\text{rad}} &= \mu_{\text{rad}} \cdot H_{\text{rad}} \\ B_{\text{tan}} &= \mu_{\text{tan}} \cdot H_{\text{tan}} \end{aligned} \tag{3}$$

  where H_{rad} and H_{tan} are the magnetic field intensities in the radial and in the circumferential direction, whereas B_{rad} and B_{tan} are the flux densities in the same directions. A linear finite element analysis is carried out and from the field solution, the radial and circumferential components of flux density (B_{rad} and B_{tan}) are extracted, as well as the radial and circumferential components of the magnetic field intensity (H_{rad} and H_{tan}). The latter are then used as input for their respective BH characteristics to calculate the actual value of μ_{rad} and μ_{tan}. The procedure continues until a convergence criterion is satisfied.

In both cases (i.e. isotropic or anisotropic) a discretization of the hysteresis region along the radial direction is performed. From the final field solution, the maximum value of the circumferential and radial components of the flux density for each discrete radius of the hysteresis region is evaluated and stored. Each of these values are the input for the hysteresis model and are used to create the corresponding minor loops. It is possible to carry out the calculation in this way because during a full revolution of one ring respect to the other, the hysteresis elements sharing the same radius will reach the same saturation level. The other inputs of the hysteresis model are the normal magnetization curve and the value of the coercive field. From these data, it is possible to estimate all the

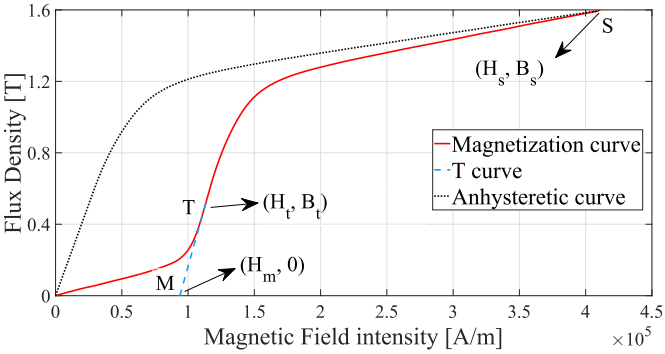

FIGURE 3. Normal magnetization curve and anhysteretic curve.

minor loops for each value of the saturation level. From (4), the actual value of the coercive field, which depends on the saturation level, is computed:

$$H_{ci} = \begin{cases} H_m + \frac{(H-H_t)}{(H_s-H_t)}(H_c - H_m) & \text{if} \quad H > H_t \\ H + \frac{(H_s-H)}{(H_s-H_{res})}H_{res} & \text{if} \quad H < H_t \end{cases} \tag{4}$$

where H is the value of the magnetic field intensity derived from the magnetostatic analysis; given the normal magnetization curve, H_m is the intercept of the tangential line at the point of maximum permeability of that curve, H_t is the value of H at the point of maximum permeability, H_c is the magnetic coercive field at the maximum saturation level and H_s is the maximum value of H and H_{res} is the value of H in the H_{an}-H plane, where H_{an} is the value of H in the anhysteresic curve, as shown in Fig. 3 . The black curve is the anhysteretic curve and represents the relationship between the values of B in the curve MTS and H_{an}. B_{MTS} is expressed by (5), whereas H_{an} can be computed by (6):

$$B_{MTS} = \begin{cases} \mu_{\max} \cdot (H_{MT} - H_t) + B_t & \text{if} \quad H < H_t \\ f(H_{TS}) & \text{if} \quad H > H_t \end{cases} \tag{5}$$

$$\begin{aligned} H_{an} &= H_{MTS} - \Delta H \\ \Delta H &= H_m \frac{H_s - H_{MTS}}{H_s - H_m} \end{aligned} \tag{6}$$

From the FE evaluated flux densities and from the actual value of the coercive field, the corresponding minor loops are computed creating a smooth curve passing through the points $(H_{ci}, 0)$, (H_p, H_p), $(-H_{ci}, 0)$ and $(-H_p, -B_p)$, as shown in Fig. 4. The minor loops are computed according to the equations presented in [25] that not reported for the sake of brevity. Clearly the accuracy of the results also depends on the procedure used to calculate the minor loops. Finally, it is possible to calculate the hysteresis energy for each component, radial and circumferential, using (7):

$$W_{\text{rad}} = \sum_{k=1}^{N} A_{\text{rad}}(k) \cdot 2\pi \cdot r(k) \cdot \frac{(r(N) - r(1))}{N}$$

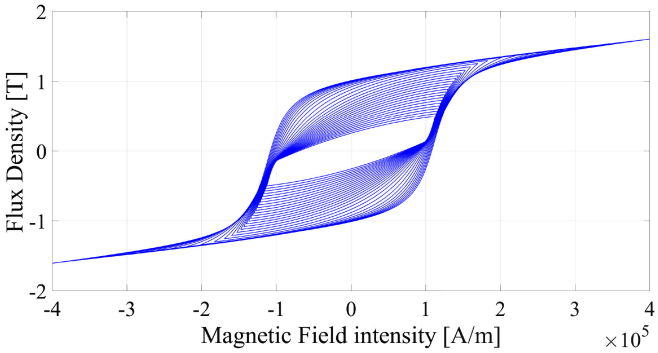

FIGURE 4. Minor loops examples generated by the adopted hysteresis model.

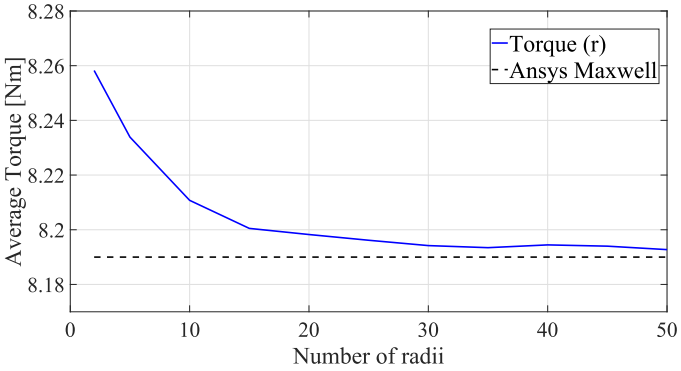

FIGURE 5. Average torque vs. number of radii.

$$W_{\tan} = \sum_{k=1}^{N} A_{\tan}(k) \cdot 2\pi \cdot r(k) \cdot \frac{(r(N) - r(1))}{N} \tag{7}$$

where $r(k)$ is the current radius of the hysteresis region, N is the number of the considered radii, $A_{\text{rad}}(k)$ and $A_{\tan}(k)$ are the areas of the hysteresis loops corresponding to the radial and circumferential components of the flux density for a certain radius k, and $\frac{(r(N)-r(1))}{N}$ is Δr. Then, the torque is calculated as:

$$T_m = \frac{n_p}{2\pi} \cdot W \tag{8}$$

where n_p is the number of pole pairs of the machine and W is the sum of W_{rad} and $W_{\tan}$. It is worth to underline that the radial and the circumferential hysteresis models are the same only in the isotropic case. Adopting this approach for the performance evaluation, the computational time is minimized without affecting the accuracy of the prediction as will be shown in the next subsection.

C. SETTING AND VALIDATION OF THE PROPOSED METHOD

With the aim of analysing the influence of the radial discretization on the performance estimation adopting the proposed method, a sensitivity analysis of a benchmark geometry has been carried out and reported in this section. The same geometry has also been analysed with a commercial FE suite (Ansys Maxwell) which is able to perform a transient FEA with a built-in vector hysteresis model. The simulated clutch (similar to the sketch reported in Fig. 1(a)) features 16 poles with the external diameter of 68 mm, whereas the hysteresis region (of Alnico 9) radial thickness is 5 mm and NdFeB-PM thickness is 3.5 mm. The geometry is meshed with approximately 26 000 nodes and 52 000 triangular elements.

As expected, the accuracy of the proposed procedure depends on the number of radial regions in which the hysteresis material is discretized, according to (7). A higher number of radii will provide a better approximation for the integral expressed by (9):

$$W_{\text{rad}} = 2\pi \int_{r_1}^{r_2} A_{\text{rad}}(r) \cdot r dr$$

TABLE 1. Comparison Between Performance Evaluation Methods

Method	Average Torque [Nm]	Simulation time [s]
Simplified method	9.15	5
Proposed method	8.21	6
Transient method	8.19	900

$$W_{\tan} = 2\pi \int_{r_1}^{r_2} A_{\tan}(r) \cdot r dr \tag{9}$$

where r_1 and r_2 are the inner radius and the outer radius of the hysteresis region.

Fig. 5 reports the average torque estimated by the proposed method as a function of the number of considered radii in the fields computation, superimposed to the average torque computed by the commercial FE software. Clearly the calculated torque reaches a plateau after the number of radii exceeds 20. Around this level of radial discretization, the error with the average torque calculated by Ansys Maxwell falls within 1%. Similar results have been obtained by analysing several other clutch geometries; they are not shown here for the sake of brevity. Table 1 summarizes the results obtained with the commercial FE suite and the proposed method along with the related computational burden. There is a two order of magnitude difference between the required simulation times, while only 1% difference in terms of calculated average torque. Consequently it would be impracticable to use such time consuming performance estimation approach within any design procedure. Table 1 also reports the torque estimation obtained with the extremely simplified case of not carrying out any radial discretization and considering the average value of the flux density along the radial thickness of the hysteresis ring as the input of the hysteresis model. Although computational-wise it is comparable, there is an error of 10% in the estimation of the torque compared to the more refined estimation achieved with 20 radial discretizations. It is worth to underline the really good agreement obtained comparing the proposed approach and the more time consuming FEA of the commercial suite. The latter implements an improved version of the vector play hysteresis model [26] which not

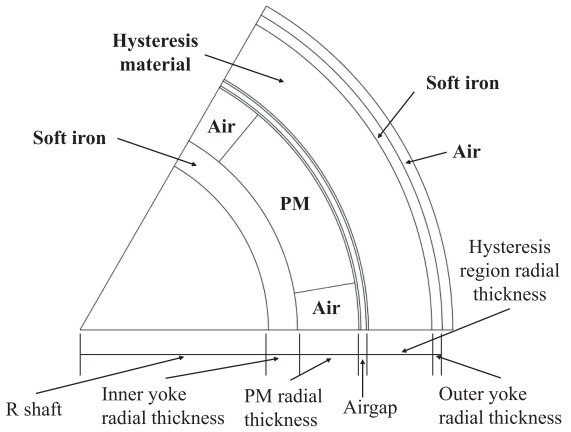

FIGURE 6. Sketch of the adopted parametrization of the hysteresis clutch.

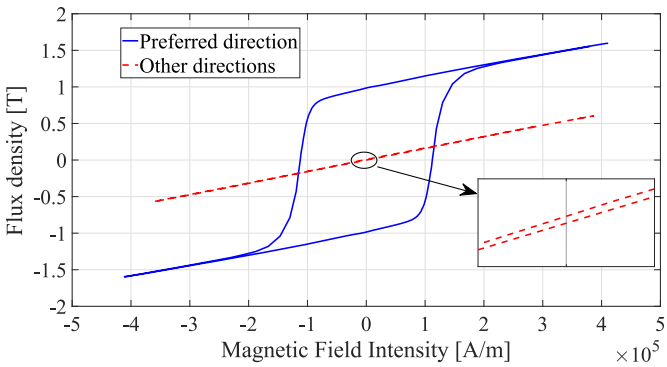

FIGURE 7. Measured major loops of AlNiCo 9 in both directions with an inset showing the dimension of the loop in the direction of low permeability.

only provides a better estimation of the hysteresis when considering alternating flux, but it is also able to take into account the effect of the rotating magnetic field on the hysteresis phenomena. The proposed approach clearly disregards such aspect during the torque computation being the radial and circumferential components of the fields separately treated. The validity of this assumption increases as the thickness of the hysteresis ring decreases; in fact for small thicknesses of hysteresis material, the magnetic field within this region can be considered either radial or circumferential [15].

IV. PROBLEM STATEMENT

The low computational burden of the proposed method of analysis, consisting in a magnetostatic finite element analysis combined with a post-processing evaluation of the hysteresis torque, makes this method suitable to be implemented within an automatic design optimization procedure. The proposed design procedure is applied considering a clutch whose external diameter is set to 68 mm and its axial length to 31.5 mm. The inner ring is made of NdFeB (N45SH) magnets and the outer hysteresis ring is made of AlNiCo 9. The goal of the design optimization is to maximize the performances (i.e. the torque T_m) and minimize the magnets volume, in order to reduce the cost of the device. The considered magnets volume V_{mag} is simply the sum of the NdFeB (V_{NdFeB}) volume and the AlNiCo volume (V_{AlNiCo}). This two objective optimization problem:

$$\min(-T_m, V_{\text{mag}}) \tag{10}$$

is solved using a stochastic optimization algorithm, the NSGA-II implemented in Matlab environment.

A. PARAMETRIZATION OF THE GEOMETRY

For the purpose of the fast evaluation of the mean torque, only one pole of the machine (depicted in Fig. 6) is considered, using anti-periodic boundary conditions. The geometric variables to identify are the split ratio, i.e. the ratio between the airgap diameter and the outer diameter, the hysteresis region radial thickness, the angular span of the NdFeB-PM, the shaft diameter and the NdFeB-PM radial thickness. The number of pole pairs is not included among the parameters varied by the optimization algorithm in order to avoid a mixed-integer stochastic optimization; indeed a single optimization is carried out for each value of poles in the range 10–30. These bounds are selected according to mechanical considerations. The geometry is parametrized in per unit in order to avoid geometrically unfeasible solutions and add further constraints and complexity to the optimization problem. In particular, the hysteresis region radial thickness is expressed in p.u. of the available space between the outer diameter and airgap diameter. The angular span of the PM is in p.u. of the polar angle, the shaft diameter is a portion of the airgap diameter while the PM radial thickness is in p.u. of the available space between the airgap diameter and the shaft diameter. The minimum radial thickness of each component is set to 0.5 mm.

B. ALNICO EXPERIMENTAL CHARACTERIZATION

As previously mentioned AlNiCo 9 is an anisotropic material whose orientation is achieved via heat treatment, i.e. by cooling it down from a temperature of about 1093 °C at a controlled rate, within a magnetic field which conforms to the preferred direction of magnetization [27]. According to the direction of the magnetic field during the heat treatment, the ring of AlNiCo 9 can show better magnetic properties in the radial or circumferential direction. Fig. 7 reports the complete measured hysteresis loops of the AlNiCo 9 in both directions. It can be clearly noticed the extreme level of anisotropy featured by the material along with the negligible dimension of the hysteresis loop area in the non-preferred direction as shown in the inset of the same figure.

C. OPTIMIZATION PROCEDURE

The selected optimization algorithm, NSGA-II, belongs to the class of biology-inspired and population-based optimization algorithms. The initial randomly generated population evolves throughout the generations by means of crossover and mutation operators. The first one tends to focus on the most promising region of the research space, i.e. the solutions showing

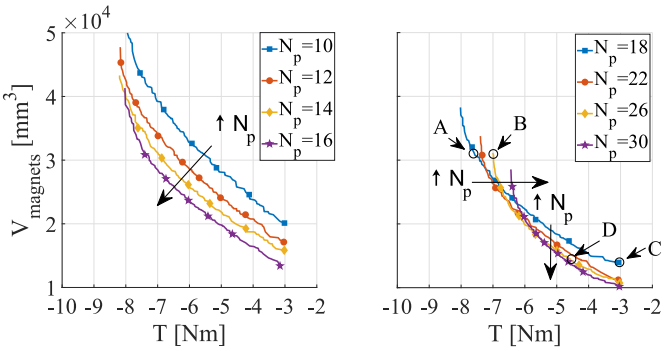

FIGURE 8. Pareto fronts: isotropic case.

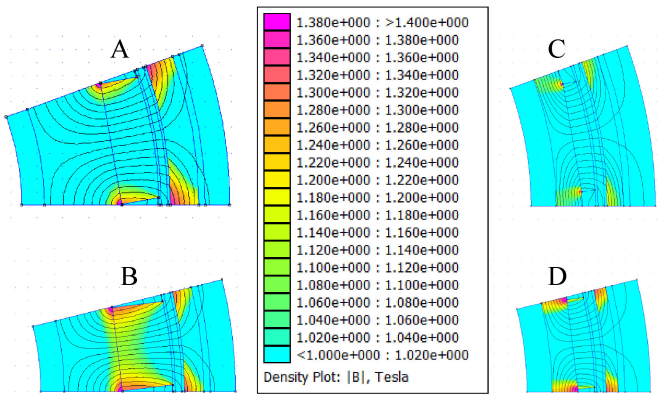

FIGURE 9. Flux densities distribution with field lines of the optimal solutions obtained considering an isotropic hysteretic material.

the best fitness while the second one tries to explore new parts of the research space. The right balance between these two mechanisms, affecting the trade-off between the exploration and exploitation of the research space, determines the effectiveness and convergence time of the optimization. The adopted algorithm also shows good performances in terms of finding a diverse set of Pareto optimal solutions [28]. Being five the number of geometrical variables to identify, a population size of 50 individuals evolving for 50 generations has been set leading to 2500 total functional evaluations per optimization. For each functional evaluation, a magneto-static finite element simulation is performed and the mean torque of the machine is calculated with the procedure outlined in the previous sections while the volume of the PMs is computed analytically. The optimization was performed on a workstation with 1600 quad-core processor running at 3.50 GHz and 16 GB of RAM. The total computational time is approximately 3 hours for the isotropic case and 21 hours for the anisotropic one. For the purpose of the optimal design, three cases are considered: isotropic case, radial anisotropic case, circumferential anisotropic case. The first configuration considers a fictitious isotropic material described by a hysteresis loop equal to that of the anisotropic AlNiCo 9 in the preferred magnetization direction. The analysis of the fictitious isotropic case is performed in order to make a comparison between isotropic and anisotropic materials sharing the same hysteresis loop area.

V. OPTIMIZATION RESULTS

A. ISOTROPIC CASE

The results of the optimizations, carried out for different number of poles (from 10 to 30), are reported in Fig. 8 in terms of Pareto fronts subdivided into two sub-figures for the sake of clarity. As expected, the overall magnets volume and the torque show a competitive behaviour, i.e. one cannot improve without the worsening of the other. Unexpectedly the torque is not always proportional to the number of poles when considering the same external dimensions of the clutch as in this case study. In fact, when considering low number of poles (10–16), an increment of the latter always produces an improvement of the performance, i.e. the same torque can be achieved with lower magnet volume or the same overall magnet volume produces more torque. A rotation of the Pareto front is then visible for poles ranging from 18 to 30. In other words, an increment of the number of poles is beneficial in the medium-low torque range whereas it is not convenient if a solution producing a higher torque is selected.

TABLE 2. Comparison Between the Optimal Clutches Designed With an Isotropic Hysteretic Material

Case	A	B	C	D
Np	18	26	18	26
T [Nm]	7.56	7.00	3.05	4.47
V_{mag} [cm^3]	30.8	30.8	13.9	13.9
V_{NdFeB} [cm^3]	16.7	21.1	5.8	7.8
V_{AlNiCo} [cm^3]	14.1	9.7	8.2	6.1
B_{avg} [T]	1.3	1.2	1.1	1.3

Clearly, as the torque increases the optimal value of the poles decreases. A qualitative explanation of this unforeseen behaviour can be deduced analyzing the flux density distribution of different clutches having the same overall magnets volume but producing different torques. Fig. 9 reports a clutch with 18 poles producing 7.5 Nm (A), and a solution with 26 poles providing 7 Nm (B). The same figure also reports two other solutions (C and D) with a low value of average torque, 3.05 Nm (18 poles) and 4.47 Nm (26 poles) respectively. The main characteristics of the selected clutches are shown in Table 2. Let us analyze the first couple of selected clutches. According to (1), the torque produced by the hysteresis clutch is proportional to the AlNiCo volume, the poles of NdFeB and the integral $\oint \mathbf{B}d\mathbf{H}$ over the AlNiCo volume. The selected clutches share the same product between number of poles and AlNiCo volume but do not provide exactly the same torque. This is mainly due to the different magnetic exploitation of the AlNiCo material in the two selected clutches. In fact, the lower poles solution guarantees a slightly better exploitation of the magnetic material being the maximum flux density higher in this case with respect to the solution with 26 poles. Conversely, comparing the solutions named C and D, the high

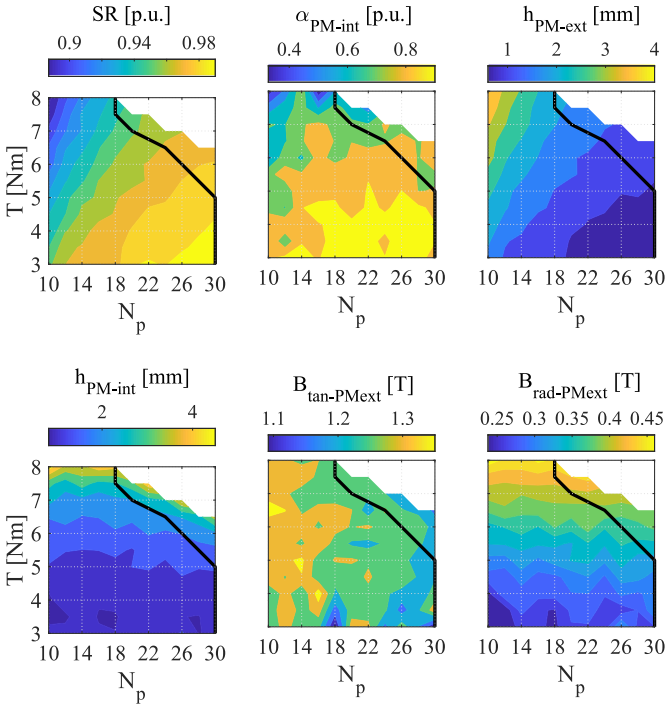

FIGURE 10. Variables trend: isotropic case.

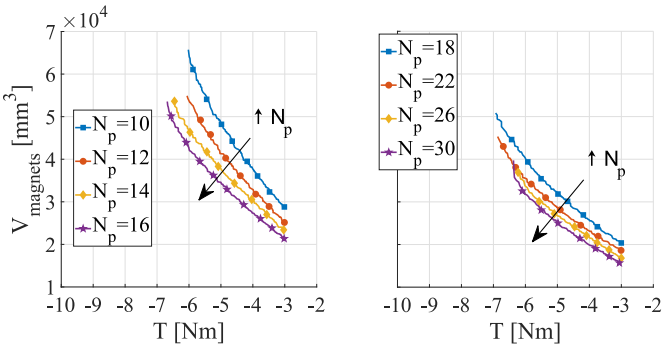

FIGURE 11. Pareto fronts: radial anisotropic case.

poles clutch allows a better exploitation of the magnetic material with respect to the 18 poles one. In fact, the average values of the flux densities in the hysteresis region are, respectively, 1.3 T and 1.1 T. It is worth to notice the opposite behaviour with respect to the A vs B comparison.

These optimizations were performed considering a magnetic outer ring yoke. Analysing the geometrical parameters of the obtained geometries can be inferred that all the optimal clutches tend to have an outer ring yoke thickness very close to the minimum allowed value (i.e. 0.5 mm). As a consequence, the outer ring yoke is highly saturated and it behaves like air and consequentially the flux paths in the hysteresis region are mainly circumferential. It can be concluded that, dealing with hysteresis clutches made with isotropic material, a non magnetic yoke of the hysteresis region should be preferred.

The trends of the optimal variable as functions of the average torque and number of poles are shown in Fig. 10; in the same figure, the optimal N_p is reported in black for each sub-figure. Analysing these figure, the following considerations can be deduced.

- The split ratio increases as the number of poles increases and as the torque decreases; this is due to the fact that the outer diameter of the clutch is kept fixed during the optimization.
- The angular span of the NdFeB magnets is globally inversely proportional to the torque; for a given target torque, it is independent on the number of poles, whereas the higher the torque the higher NdFeB magnets height (h_{PM-int}).
- The radial thickness of the AlNiCo region (h_{PM-ext}), which defines the AlNiCo volume, shows the opposite trend with respect to the split ratio. In fact, it increases with the torque and decreases with the number of poles.
- The mean value of the circumferential flux density ($B_{tan-PMext}$) in the hysteresis region is higher than the radial one, due to the saturation of the magnetic yoke which forces the flux lines in the circumferential direction.
- Being the AlNiCo BH curve knee approximately 1.2 T, the material reaches the saturation in the circumferential direction, especially for low number of pole pairs. As a consequence, part of the magnetic flux is in the radial direction and this has a minor effect on the torque production which becomes more evident in the high torque range as will be discussed in Section V-D.

B. RADIAL ANISOTROPIC CASE

Fig. 11 reports the optimization results obtained considering the hysteresis material (AlNiCo 9) with the preferred direction of magnetization along the radial direction. Unlike the isotropic case, there is no rotation of the Pareto fronts with respect to the number of poles. As a consequence, the torque increases monotonically with the number of poles. The maximum torque is 6.8 Nm with a magnets volume of $3.2 \cdot 10^4$ mm^3, so there is a torque reduction of 8.5% and a volume increase of 40% with respect to the isotropic case. Analysing the variables trend reported in Fig. 12 which shows their contour plot, the following consideration can be done.

- The split ratio is globally torque independent and it is proportional to the number of poles.
- For a given torque value, the number of poles has a limited influence on the optimal angular span.
- The radial thickness of the NdFeB and AlNiCo parts show the same trend as in the isotropic case.
- Regarding the magnetic fields, since the preferred direction is the radial one, the circumferential flux density is very low and it basically does not contribute to the torque production. Conversely, the mean value of the radial component is independent on the torque and it is inversely proportional to the number of poles.

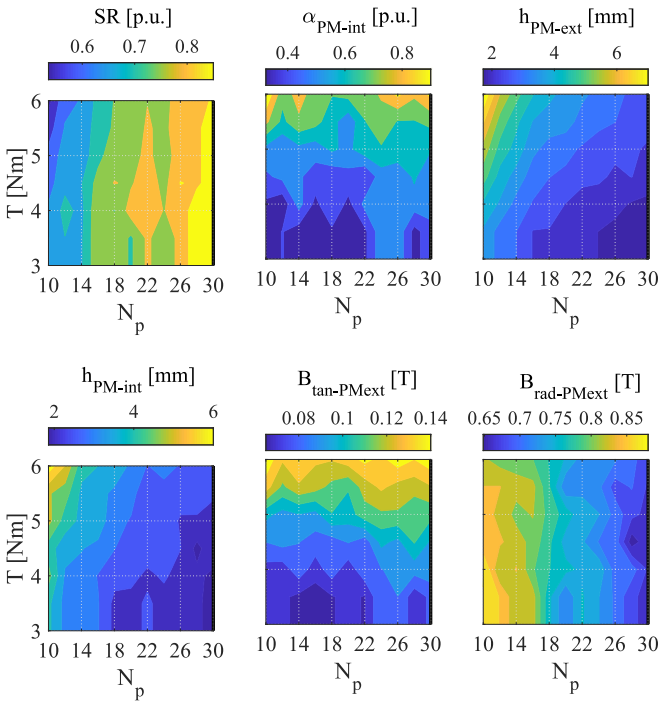

FIGURE 12. Variables trend: radial anisotropic case.

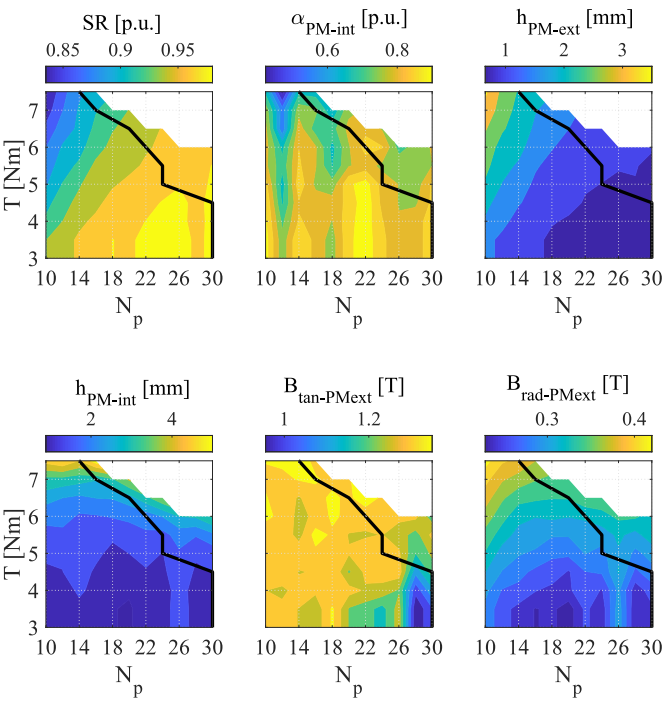

FIGURE 14. Variables trend: circumferential anisotropic case.

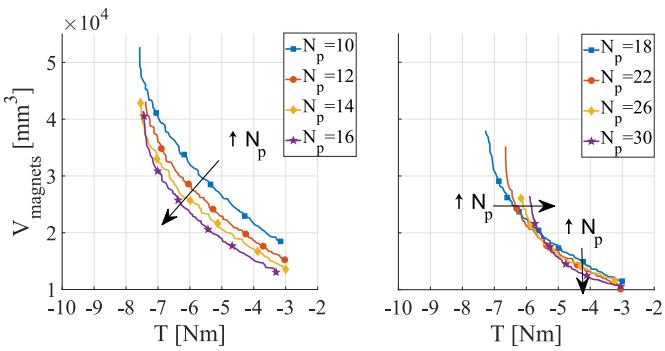

FIGURE 13. Pareto fronts: circumferential anisotropic case.

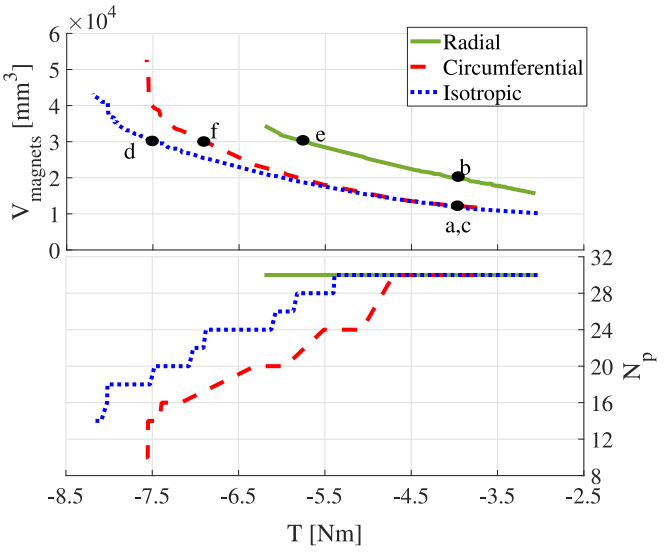

FIGURE 15. Comparison among the optimal results achieved considering isotropic and circumferential and radial anisotropic material.

The fact that the hysteresis material does not reach the saturation suggests a worsen magnetic exploitation of the available space compared to the the isotropic case leading to a reduction of the maximum achievable torque.

C. CIRCUMFERENTIAL ANISOTROPIC CASE

Fig. 13 shows the results of the circumferential anisotropic case. As for the isotropic case, a rotation of the Pareto fronts is evident in the 18–30 poles range. The maximum reached torque in the circumferential anisotropic case is 7.5 Nm, with a corresponding magnets volume of $3.5 \cdot 10^4$ mm^3. Concerning the variables (Fig. 14), it is worth to notice that:

- the split ratio, the angular span of the NdFeB magnets and the radial thickness of the NdFeB magnets and the hysteresis region globally exhibit the same trend of the isotropic case;
- the mean value of the flux density in the circumferential direction is bounded between 1 T and 1.3 T.

D. COMPARISON AND CONSIDERATIONS

Starting from the Pareto fronts obtained in the previous subsections, the overall front for each case has been determined and they are shown in Fig. 15 along with the optimal number of poles. As previously mentioned, the radial anisotropic case clearly shows worst performance respect to the other two cases. The isotropic and circumferential anisotropic cases

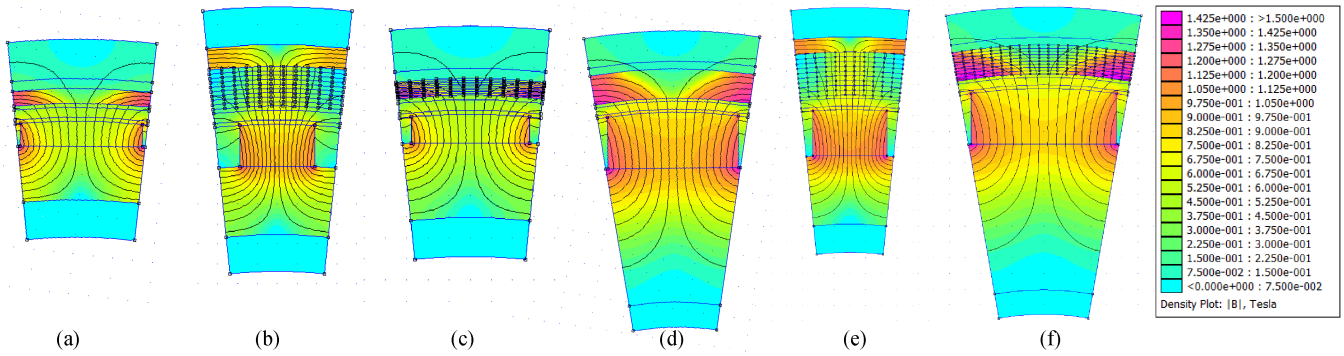

FIGURE 16. Flux density distributions with field lines of the optimal geometries producing the same torque (a, b, c) or having the same overall magnet volume (d, e, f). Respectively a) and d) show the isotropic scenario, b) and e) the radial anisotropic ones while c) and f) the circumferential anisotropic cases.

TABLE 3. Comparison Between the Selected Clutches

Case	a	b	c	d	e	f
Np	30	30	30	20	30	18
T [Nm]	4	4	4	7.45	5.67	6.93
V_{mag} [cm^3]	12.1	20.1	12.1	30	30	30
V_{NdFeB} [cm^3]	7.2	7.5	6.9	17.9	12.9	18.1
V_{AlNiCo} [cm^3]	4.9	12.5	5.2	12.1	17.1	11.9
V_{NdFeB}/V_{AlNiCo}	1.47	0.59	1.33	1.47	0.76	1.52

present the same behaviour in the low-medium torque range, while differ for high torques. In particular the isotropic case performs better respect to the circumferential anisotropic case because, for higher torques, the flux density in the circumferential direction reaches the saturation. At this point, in the isotropic clutch, the radial flux density is exploited to increase the torque, whereas in the anisotropic one, the radial flux density does not produce torque and so the latter cannot be increased. While for the radial anisotropic case increasing the number of poles is always beneficial, this is not true for the other two cases as shown in Fig. 15. In particular, the optimal number of poles decreases as the target torque increases for both isotropic and circumferential anisotropic hysteretic materials. In addition, the optimal pole counts of the isotropic case in the medium-high torque range is higher respect to the circumferential anisotropic variant. The latter behaviour is mainly due to the possibility of the isotropic version to exploit also the radial component of the magnetic flux density.

A number of clutches sharing the same torque (4 Nm) or the same overall magnet volume (30 cm^3) are analyzed in details. Table 3 reports the main parameters of the selected geometries. Fig. 16(a), 16(b) and 16(c) report the geometries and the flux density maps for the three clutches sharing the same average torque. It is worth to notice that the radial anisotropic hysteresis clutch is far from being saturated differently than the isotropic and circumferential anisotropic ones. Due to the geometric constraints, if the flux paths are mainly circumferential, the flux density in the hysteresis region increases with respect to the radial case. In fact, for a given magnetic flux passing through the airgap, the section of the hysteresis region crossed by the flux lines increases in the radial anisotropic case. So, the flux density, which is inversely proportional to the section, decreases. Considering the same external diameter, radial hysteresis clutches need a non saturated external yoke and a bigger hysteresis region leading to a smaller airgap radius with respect to the circumferential cases. This produces a further torque reduction. As a consequence, to reach the same torque the AlNiCo volume of the radial clutch is almost doubled with respect to the isotropic and circumferential cases, whereas the NdFeB volume barely changes. Analysing the quotas of the NdFeB and the AlNiCo volumes in the three cases, it can be inferred that for optimal radial clutches the Alnico quantity is higher respect to the NdFeB one; the opposite happens for the other two types of clutches. Fig. 16(d), 16(e) and 16(f) report the geometries and the flux density contour plots for the three selected clutches sharing the same magnets volume. For the considered overall magnets volume, the radial clutch presents a torque reduction with respect to the isotropic and circumferential ones equal to 25% and 18%, respectively. In this case, the above reported consideration regarding the V_{NdFeB} to V_{AlNiCo} ratio are even more evident as reported in the last row of Table 3. Consequentially it can be stated, that in order to improve the performances of a radial flux type hysteresis clutch is better to have a higher AlNiCo volume respect to the NdFeB one. This is mainly due to the fact that once the maximum value of the flux density in the hysteresis region is reached, a further increment of the NdFeB volume does not produce a significant torque improvement. The same does not hold for the isotropic or the circumferential flux clutch topologies where the overall magnet volume is mainly made of NdFeB.

The optimization results can be used to draw design guidelines for hysteresis clutches; in fact according to the type of the HFM (i.e isotropic or anisotropic) the following considerations can be drawn.

- For a given area of the hysteresis loop, an isotropic material performs better than an anisotropic one. However, isotropic materials usually show a smaller hysteresis loop with respect to the anisotropic ones. For example, the coercive field of AlNiCo 4 (which is one of the strongest isotropic AlNiCo) is 57 kA/m, whereas the one of the AlNiCo 9 is 109 kA/m. Consequentially the optimal performance achievable with a real isotropic Alnico will be worse respect to the ones shown with the blue line in Fig. 15.
- If the HFM is isotropic, the outer yoke must be non-magnetic in order to force the flux lines in the circumferential direction. This lead to an improvement of the torque for a given outer envelope.
- If the HFM is anisotropic, in order to increase the average torque, the preferred magnetization direction should be the circumferential one.
- The number of poles is not always proportional to the torque but depends on the hysteresis clutch type. Radial type hysteresis clutches feature a direct proportionality between torque and poles, whereas this does not hold for the other types of analyzed clutches. This behaviour can be explained by the different magnetic exploitation of the available space of the three considered topologies. The radial type ones never reach the saturation of the hysteresis region, therefore their working points lie always in the linear region. The other two topologies easily reach the knee of the BH curve of the HFM and so, after a certain point, an increase in the poles number does not produce a torque improvement. This result is more evident analyzing Fig. 15 which also reports the optimal pole counts as function of the torque.
- The V_{NdFeB} to V_{AlNiCo} ratio should be less than one if a radial flux type hysteresis is considered, whereas a ratio greater than one is preferable in a circumferential flux hysteresis machine.

VI. CONCLUSION

This paper has presented an accurate and fast method of design and analysis of hysteresis clutches. The proposed approach to the analysis does not require the implementation of complex hysteresis models and it is applicable both to isotropic and anisotropic materials. It is constituted by a magneto-static FE simulation followed by a post processing of the magnetic field in order to evaluate the average torque. The low computational burden and the ease of implementation make the proposed technique suitable for automatic design optimization. The proposed procedure has been implemented via an open-source FE software and the Matlab platform therefore it does not require commercial FE solvers. A comprehensive design procedure aided by stochastic optimization algorithms has been outlined in order to maximize the average torque and minimize the magnets volume for a given outer diameter and axial length. Several optimizations have been performed considering different number of poles and magnetic material properties including the preferred direction of magnetization of the hysteretic material. Analyzing the output of the multi-objective optimization, i.e. a set of non-dominated solutions, it has been possible to draw general design guidelines of hysteresis clutches.

REFERENCES

[1] J. Yoo, S. Yang, and J. S. Choi, "Optimal design of an electromagnetic coupler to maximize force to a specific direction," *IEEE Trans. Magn.*, vol. 44, no. 7, pp. 1737–1742, Jul. 2008.

[2] L. Belguerras, S. Mezani, and T. Lubin, "Analytical modeling of an axial field magnetic coupler with cylindrical magnets," *IEEE Trans. Magn.*, to be published, doi: 10.1109/TMAG.2020.3005949.

[3] C. Steinmetz, *Theory and Calculation of Alternating Current Phenomena*, vol. 4 McGraw-Hill Book Company, Incorporated, 1916.

[4] R. Galluzzi, N. Amati, and A. Tonoli, "Modeling, design, and validation of magnetic hysteresis motors," *IEEE Trans. Ind. Electron.*, vol. 67, no. 2, pp. 1171–1179, Feb. 2020.

[5] A. A. Nasiri, M. Mirsalim, and A. R. Nasiri, "A novel hybrid hysteresis motor with multi-stack PM-hysteresis rotor; general modeling, analysis and design optimization," in *Proc. Int. Power Syst. Conf.*, 2019, pp. 150–158.

[6] K. R. Rajagopal, "Design of a compact hysteresis motor used in a gyroscope," *IEEE Trans. Magn.*, vol. 39, no. 5, pp. 3013–3015, Sep. 2003.

[7] B. R. Teare, "Theory of hysteresis-motor torque," *Elect. Eng.*, vol. 59, no. 12, pp. 907–912, 1940.

[8] M. A. Copeland and G. R. Slemon, "An analysis of the hysteresis motor i - analysis of the idealized machine," *IEEE Trans. Power App. Syst.*, vol. 82, no. 65, pp. 34–42, Apr. 1963.

[9] Hong-Kyu Kim, Sun-Ki Hong, and Hyun-Kyo Jung, "Analysis of hysteresis motor using finite element method and magnetization-dependent model," *IEEE Trans. Magn.*, vol. 36, no. 4, pp. 685–688, Jul. 2000.

[10] R. Nasiri-Zarandi and M. Mirsalim, "Finite-element analysis of an axial flux hysteresis motor based on a complex permeability concept considering the saturation of the hysteresis loop," *IEEE Trans. Ind. Appl.*, vol. 52, no. 2, pp. 1390–1397, Mar./Apr. 2016.

[11] J. B. Padilha, P. Kuo-Peng, N. Sadowski, and N. J. Batistela, "Vector hysteresis model associated to FEM in a hysteresis motor modeling," *IEEE Trans. Magn.*, vol. 53, no. 6, pp. 1–4, 2017.

[12] G. Gallicchio, M. Palmieri, M. Di Nardo, and F. Cupertino, "Fast torque computation of hysteresis motors and clutches using magneto-static finite element simulation," *Energies*, vol. 12, no. 17, p. 3311, Aug. 2019.

[13] D. Jiles, *Introduction to Magnetism and Magnetic Materials*, 2nd ed. New York, NY, USA: Taylor & Francis, 1998. [Online]. Available: https://books.google.co.uk/books?id=axyWXjsdorMC

[14] K. Kurihara, N. Kurihara, and T. Kubota, "Torque analysis of the hysteresis motor with over-excitation using play model," in *Proc. 22nd Int. Conf. Elect. Mach. Syst.*, 2019, pp. 1–6.

[15] A. Canova and F. Cavalli, "Design procedure for hysteresis couplers," *IEEE Trans. Magn.*, vol. 44, no. 10, pp. 2381–2395, Oct. 2008.

[16] T. M. Vorob'yeva, *Electromagnetic Clutches and Couplings. International Series of Monographs on Electronics and Instrumentation*. New York: Pergamon, US, 1965.

[17] H. C. Roters, "The hysteresis motor-advances whick permit economical fractional horsepower ratings," *Trans. Amer. Inst. Elect. Eng.*, vol. 66, no. 1, pp. 1419–1430, 1947.

[18] A. Maxwell, Ansys Maxwell Documentation. 2019. Accessed: May 9, 2020. [Online]. Available: http://www.ansys.com

[19] COMSOL., COMSOL Multiphysics Documentation. 2017. Accessed : Apr. 7, 2020. [Online]. Available: http://www.comsol.com

[20] D. Lin, P. Zhou, C. Lu, N. Chen, and M. Rosu, "Construction of magnetic hysteresis loops and its applications in parameter identification for hysteresis models," in *Proc. Int. Conf. Elect. Mach.*, 2014, pp. 1050–1055.

[21] D. C. Jiles, J. B. Thoelke, and M. K. Devine, "Numerical determination of hysteresis parameters for the modeling of magnetic properties using the theory of ferromagnetic hysteresis," *IEEE Trans. Magn.*, vol. 28, no. 1, pp. 27–35, Jan. 1992.

[22] S. Willerich and H. Herzog, "A continuous vector Preisach model based on vectorial relay operators," *IEEE Trans. Magn.*, vol. 56, no. 3, pp. 1–4, Mar. 2020, Art no. 7511204.

[23] L. Zhu *et al.*, "An improved anisotropic vector preisach hysteresis model taking account of rotating magnetic fields," *IEEE Trans. Magn.*, vol. 55, no. 6, pp. 1–4, Jun. 2019, Art no. 7300404.
[24] D. Meeker, "Finite element method magnetics," Feb. 5, 2009, Ver.4.2 user's manual. [Online]. Available: http//www.femm.info/Archives/doc7manual.pdf
[25] D. Lin, P. Zhou, C. Lu, N. Chen, and M. Rosu, "Construction of magnetic hysteresis loops and its applications in parameter identification for hysteresis models," in *Proc. Int. Conf. Elect. Mach.*, 2014, pp. 1050–1055.
[26] D. Lin, P. Zhou, and A. Bergqvist, "Improved vector play model and parameter identification for magnetic hysteresis materials," *IEEE Trans. Magn.*, vol. 50, no. 2, pp. 357–360, Feb. 2014, Art no. 7008704.
[27] Arnold, "Cast Alnico Permanent Magnet Brochure," Accessed: Mar. 22, 2020. [Online]. Available: http://www.arnoldmagnetics.com/wp-content/uploads/2017/10/Cast-Alnico-Permanent-Magnet-Brochure-101117-1.pdf
[28] K. Deb, A. Pratap, S. Agarwal, and T. Meyarivan, "A fast and elitist multiobjective genetic algorithm: NSGA-II," *IEEE Trans. Evol. Comput.*, vol. 6, no. 2, pp. 182–197, Apr. 2002.

GIANVITO GALLICCHIO (Member, IEEE) received the B.Sc. (Hons.) and M.Sc. (Hons.) degrees in electrical engineering from the Politecnico di Bari, Bari, Italy, in 2016 and 2018, respectively. He is currently working toward the Ph.D. degree with the Electrical Machines and Drives Group, Politecnico di Bari, Bari, Italy. His main research interests include the analysis, modelling and design of magnetic couplers for industrial applications and the design of electrical machines, including permanent magnet and reluctance synchronous machines, for aerospace sector.

MAURO DI NARDO (Member, IEEE) received the M.Sc. (Hons.) degree in electrical engineering from the Polytechnic University of Bari, Italy, in 2012, and the Ph.D. degree in electrical machine design from the University of Nottingham, U.K., in 2017. From 2017 to 2019, he was Head with the AROL Research Team within the Polytechnic University of Bari leading industrial R&D projects on electrical drives design for mechatronics applications. Since the 2019, he was with the Power Electronics and Machine Control Group of the University of Nottingham as Research Fellow. His research interests include the analysis, modeling, and optimizations of electrical machines, including permanent magnet and synchronous reluctance topologies for automotive and aerospace sectors as well as induction motor for industrial applications.

MARCO PALMIERI (Member, IEEE) received the M.Sc. and Ph.D. degrees in electrical engineering from Politecnico di Bari, Bari, Italy, in 2011 and 2016, respectively. Since 2017, he has been with the Department of Electrical and Information Engineering, Politecnico di Bari, where he is currently a Postdoc Researcher. From 2011 to 2015, he was with the Energy Factory Bari Research Team, working on high-speed electrical machines for aeronautical applications. In 2014, he was with the Power Electronics, Control, and Machines Research Group of the University of Nottingham, working on electrical machines for aeronautical applications. In 2019, he was Visiting Researcher with the Laboratory of Actuation Technology of the Saarland University. His research interests include the design of high-speed electrical machines by means of optimization algorithms and finite element analysis. He Co-received the Prize Paper Award from the IEEE Industrial Electronics Society Electrical Machines Committee in 2015.

FRANCESCO CUPERTINO (Senior Member, IEEE) received the Laurea and Ph.D. degrees in electrical engineering from the Politecnico di Bari, Bari, Italy, in 1997 and 2001, respectively. Since 2001, he has been with the Department of Electrical and Information Engineering, Politecnico di Bari, Bari, Italy, where he is currently a Full Professor of converters, electrical machines, and drives. He is the Scientific Director of four public/private laboratories with Politecnico di Bari that enroll more than 50 researchers, the laboratory Energy Factory Bari, with GE AVIO, aimed at developing research projects in the fields of aerospace and energy, the More Electric Transportation laboratory, with CVIT SpA (BOSCH Group), aimed at developing technologies for sustainable mobility, Cyber Physical Systems AROL Bari, with AROL SpA, focused on closure systems for food and beverage, Innovation for Mills, with Casillo Group and Idea75, focused in the Industry4.0 applications for wheat processing. He has authored or coauthored more than 130 scientific papers on these topics. His research interests include the design of synchronous electrical machines, motion control of high performances electrical machines, applications of computational intelligence to control, and sensorless control of ac electric drives. He was the recipient of the two best paper awards from the Electrical Machines Committee of the IEEE Industry Application Society and from the homonymous Committee of the IEEE Industrial Electronics Society, in 2015. He is currently the rector of Politecnico di Bari.